Degradation of a water-in-salt electrolyte at graphite and Na metal electrodes from first principles

Majid Rezaei[1,*] *and Axel Groß*[1,2]

[1]Institute of Theoretical Chemistry, Ulm University, Oberberghof 7, 89081 Ulm, Germany

[2]Helmholtz Institute Ulm (HIU) for Electrochemical Energy Storage, Helmholtzstraße 11, 89069 Ulm, Germany

Abstract

By preventing water decomposition on the electrode surface, the solid-electrolyte interphase (SEI) plays a crucial role in enhancing the electrochemical stability of water-in-salt electrolytes, thereby facilitating their commercialization. In this study, we employ density functional theory calculations to explore the initial stages of SEI formation within a sodium triflate water-in-salt electrolyte on two types of electrodes: graphite, known for its inert characteristics, and a highly reactive sodium metal surface, both commonly used in sodium-ion batteries. The insights gained from our calculations offer predictive information on the potential composition of the interfacial layer forming on these surface models, shedding light on the electrochemical performance of the system as a battery feature.

1. Introduction

While Li-ion batteries offer high performance in terms of energy density, operating voltage, and cycle life [1, 2], they cannot meet the growing demand for energy storage alone, primarily due to the relative scarcity of lithium resources [3]. Additionally, concerns exist regarding their physicochemical performance [4], safety [5], sustainability of the materials used [6], and environmental impact both during lithium mining [3, 7] and after battery disposal [8]. Therefore, it is essential to explore alternative energy storage systems to address these limitations and

* Corresponding author - Email: majid.rezaei@uni-ulm.de

concerns. Recently, Na-ion batteries have emerged as one of the most promising alternatives [9-15], primarily due to the abundance and widespread distribution of their raw materials and their relatively low production costs [16]. Additionally, since sodium exhibits similar chemical behavior to lithium, many mechanisms and components developed for Li-ion batteries can be adapted for Na-ion batteries [17], facilitating initial progress toward their commercialization. However, serious challenges remain for this type of battery, including limited energy densities, power rates, and cycle lives compared to Li-ion batteries [18], as well as potential safety concerns similar to those associated with Li-ion batteries.

Addressing the challenges of Li-ion and post-Li-ion batteries, including Na-ion variants, requires improvements in both electrolyte and electrode materials. This necessitates detailed studies of the system behavior in both the bulk liquid and solid phases, as well as the solid-electrolyte interphase (SEI). In Na-ion batteries, the solid phase typically features hard carbon as the anode material, while the cathode is commonly made from Prussian blue/white and their analogues, layered transition metal oxides, or vanadium phosphate [10, 19-22]. Regarding the liquid phase, carbonate-based organic electrolytes have been proposed, often with small amounts of additives that help stabilize the SEI on anode and cathode during cycling [23-27]. However, these electrolytes share similar safety concerns with Li-ion batteries due to the presence of highly flammable organic carbonates [28]. Non-flammable ionic liquids [29] address this safety risk while also offering a sufficiently wide electrochemical stability window, excellent thermal stability, and low vapor pressure [30-37]. However, they are typically constrained by high production costs [38] and relatively low ionic conductivity [39]. As an alternative, water-in-salt (WiS) electrolytes have recently gained attention [40-42]. Although these electrolytes may provide lower electrochemical stability compared to ionic liquids, they benefit from reduced production costs by using water, the most abundant solvent in nature, and excellent transport properties that often surpass those of ionic liquids [43]. Additionally, their nonflammable nature ensures high

safety, similar to ionic liquids, making them promising candidates for advanced energy storage systems with enhanced safety requirements.

While many experimental and computational studies have elucidated the main electrochemical processes occurring in bulk electrodes [2, 44] and bulk electrolytes [43, 45], the complex reactive behavior at the interface remains unclear. In particular, the formation mechanism and structural properties of the SEI, a crucial component that significantly impacts electrochemical stability [46] and charge/discharge processes [47], are not yet fully understood. Although early studies have provided insights into SEI quality through performance measurements [48], they lack detailed molecular-scale information on the SEI characteristics. Subsequent research utilized various ex situ techniques, such as vibrational and photoelectron spectroscopy and microscopy methods, alongside computational approaches like molecular dynamics (MD) simulations, to further investigate SEI structure in various electrolytes, with a particular focus on ionic liquids [49-51]. While these studies offer insights into the SEI composition, they lack information on the SEI formation process, particularly in its initial stages. To address this gap, Forster-Tonigold et al. [52] combined their experimental measurements with density functional theory (DFT) calculations to investigate the interactions between the 1-butyl-1-methylpyrrolidinium bis(trifluoromethane-sulfonyl)imide (BMP-TFSI) ionic liquid and bulk-like sodium and magnesium films. This approach provided an atomic-scale perspective on the reactive interactions between the examined ionic liquid and the anode models, elucidating the initial stage of SEI formation. Similarly, Stottmeister and Groß [53] employed ab initio molecular dynamics simulations based on DFT calculations to study the early stages of SEI formation during the decomposition of typical solvent molecules on alkaline metal anodes. Building on these insights, further research is needed to investigate SEI composition and formation processes across various electrolyte/electrode systems, including promising variants of WiS electrolytes, to optimize the performance of Na-ion batteries.

In a previous study [43], we employed first-principles-based MD simulations to demonstrate the potential of sodium triflate (NaOTF) WiS electrolyte for use in Na-ion batteries. This study highlighted how NaOTF provides a balance between bulk transport properties and ion-ion correlations in the bulk liquid, with the latter playing a crucial role in enhancing electrochemical stability through the formation of a stable SEI. In the present study, we extend our research to investigate the initial stages of SEI formation in the same electrolyte. To this end, we apply the DFT approach proposed by Forster-Tonigold et al. [52] to examine the interfacial interactions between the electrolyte and two distinct types of electrodes: graphite, typical of conventional carbon-based electrodes in sodium-ion batteries, and a reactive sodium metal electrode, representing either a bulk electrode or a thin film grown on the electrode surface. The primary objective of this study is to elucidate the potential mechanisms underlying the onset of SEI formation and the composition of the resulting interfacial layer covering the electrode surface. By separately analyzing aggregated and solvated ion structures, our results and conclusions can also be extended to similar ionic liquids.

2. Computational methodology

As mentioned earlier, the present study aims to analyze the solid-electrolyte interactions at the early stages of SEI formation. Our analysis focuses on the NaOTF WiS solution, a promising electrolyte for Na-ion battery applications, and models the adsorption of various electrolyte components on either graphite or sodium metal electrodes. To this end, we examine the possible ion-ion and ion-water structures present at the high salt concentrations associated with a WiS regime. As detailed in our previous study [43], at these concentrations, the NaOTF WiS electrolyte consists of two distinct domains: an ion-rich domain, primarily composed of aggregated ions, and a water-rich domain containing either partly or fully solvated ion pairs. To explore the adsorption behavior of potential aggregated ion structures, we separately model adsorption complexes containing a single NaOTF ion pair, a single Na_2OTF structure, and a single

$NaOTF_2$ structure, each in the absence of water. Although this approach neglects some details of mutual interactions in real-world large aggregates, configurations examined effectively represent the major sub-structures within the ion-rich domain. For the water-rich domain, we model both a contact ion pair, where the partly solvated cation and anion are in direct contact, and a solvent-separated ion pair, where both ions are fully solvated but share a portion of their solvation shells. These two structures are modeled as single ion pairs surrounded by an adequate number of water molecules, as discussed in section 4.3.

Since the geometry optimization may converge to various local energy minima based on the initial ion orientation, we repeat the optimization process for each system while varying the initial configuration of the OTF^- anion(s) relative to both the sodium cation(s) and the electrode surface. Subsequently, we identify the geometry with the lowest overall energy as the optimal configuration and calculate the adsorption energy based on this configuration as

$$E_{ad} = E_{tot} - E_{surf} - E_{ions} \quad (1)$$

where E_{tot} is the total energy of the adsorption complex, E_{surf} is the energy of the bare surface modeled in the same simulation cell as for the entire adsorption complex, and E_{ions} is the energy of the respective electrolyte component simulated in the gas phase within a large simulation box of $32 \times 32 \times 32$ Å^3.

To understand the decomposition behavior of triflate anions during the adsorption process, we follow the procedure outlined in Refs. [52, 54]. For this purpose, we selectively break interatomic bonds and model the resulting decomposition products on top of the electrode surface for each of the examined systems. Subsequently, we calculate the decomposition reaction energy as

$$\Delta E_{dec} = E_{decomposed} - E_{intact} \quad (2)$$

where $E_{decomposed}$ and E_{intact} represent the energies of the adsorption complexes with decomposed and intact anions, respectively. It is important to note that our analysis exclusively

focuses on the driving force for potential decomposition reactions, neglecting kinetic barriers. Nevertheless, following the Brønsted–Evans–Polanyi principle, a linear correlation between activation energies and reaction enthalpies can be approximated [52, 55]. Therefore, when comparing different reactions of similar types, the calculated reaction energies offer initial insights into their relative probabilities.

We also apply the approach described above to approximate the energy change during the partial desolvation of contact ion pairs and solvent-separated ion pairs upon their adsorption. To achieve this, we initially simulate the fully solvated structures of either contact or solvent-separated ion pairs close to the electrode surface to model their proximity to the surface. Subsequently, in the resulting optimal structure, we adjust the positions of the water molecules situated between the ions and the surface atoms to enable direct ion-surface contact. Using these modified configurations as input, we then repeat our DFT calculations to approximate the energy of the partially desolvated species adsorbed on the surface. Finally, we compare the energies of the adsorption complexes with and without partial loss of ion solvation shells

$$\Delta E_{des} = E_{solvated} - E_{desolvated} \quad (3)$$

where $E_{solvated}$ and $E_{desolvated}$ are the energies of the fully and partially solvated ion pairs, respectively.

As a critical factor influencing the electrochemical stability of the system, we also explore the probability of water decomposition upon adsorption on the surfaces. This involves selectively breaking two O-H bonds from two adjacent water molecules and examining the energetic favorability of the corresponding water reduction reaction:

$$2H_2O(l) + 2e^- \rightarrow 2OH^-(aq) + H_2(g) \quad (4)$$

where (l), (aq), and (g) represent the liquid, aqueous, and gas phases, respectively. To determine the corresponding water decomposition energy, we use Eq. 2 and reference the

respective adsorption complexes containing intact water molecules.

While the methodology described above provides valuable insights into the relative stability of different adsorption configurations by approximating adsorption or decomposition energies, it is important to acknowledge the inherent limitations of the DFT model used in our simulations (the model is outlined in section 3). Firstly, we derive only the total energies, neglecting temperature-dependent entropic contributions to the energy calculations. Secondly, the high computational cost of DFT calculations restricts the number of atoms that can be modeled and thus the complexity of the configurations that can be explored. Thirdly, this study does not explore any dynamic processes. To address these limitations, future studies could utilize MD simulations to provide further insights into the formation process and structure of the SEI. Lastly, we neglect any electrode potential effects in the adsorption. However, grand-canonical calculations have shown that these effects can often be disregarded at metal electrodes due to the good screening properties of metals [56-58].

3. Simulation setup

We conduct DFT electronic structure calculations combined with a geometry optimization scheme to obtain the optimal adsorption structures and their respective energies. Our calculations are performed using the periodic DFT package VASP [59], employing a conjugate gradient algorithm [60] to relax the geometry. For this purpose, the wave functions are expanded up to a cutoff energy of 520 eV using a plane wave basis set, and the electronic cores are described by the projector augmented wave (PAW) method [61]. The electronic structure calculations are considered converged within 10^{-6} eV, and the geometry optimizations are conducted until the forces on atoms are less than 0.01 eV/Å. The exchange-correlation energies are treated within the generalized gradient approximation, employing a revised version of the Perdew-Burke-Ernzerhof (RPBE) functional, as proposed by Hammer and Nørskov [62]. To account for dispersion effects, we employ the semi-empirical D3 dispersion correction scheme

of Grimme with the zero damping function [63-65], which is effective for modeling a broad range of relevant systems [66]. In our analysis, this D3 dispersion correction combined with the RPBE exchange-correlation functional yields accurate predictions for a bulk graphite system concerning both the interlayer distance in the stacking direction and the interlayer binding energy, as indicated in Table S1.

To optimize computational efficiency while ensuring accuracy, we conduct an initial test analysis by increasing the number of k-points for integration over the first Brillouin zone and the number of surface layers. Additionally, we test different PAW potentials for sodium with varying valence configurations. The respective results are provided in Table S2. Based on this analysis, we adopt a (2×2×1) k-point mesh in all our subsequent calculations, as it offers sufficient accuracy for both the adsorption energy and the resulting structural properties. Moreover, in all our subsequent simulations, the graphite surface is modeled by three atomic layers, and the sodium surface is modeled by four atomic layers. For the sodium cation adsorbing on the graphite surface, we utilize the PAW potential including 9 valence electrons ($2S^2 2P^6 3S^1$). This choice offers better convergence in the electronic structure calculations, leading to reduced runtime. For simulations involving the sodium metal surface, we employ the PAW potential with 1 valence electron ($3S^1$) for sodium, which provides sufficient accuracy and a significantly lower computational expense.

We utilize the AB stacking configuration for graphite, recognized as the most stable graphite configuration[67], while representing the sodium surface in both bcc (100) and hcp (0001) lattices. For all the examined surface models, a vacuum region of approximately 29 Å is included between the surface and its periodic image in the direction perpendicular to the surface. The atoms in the lowest layer of each surface are fixed to their initial positions to mimic bulk-like behavior, while the other surface layers are allowed to relax during the geometry optimization process. To investigate the adsorption of various electrolyte components

on the sodium metal surfaces and different aggregated ion structures on the graphite surface, we employ (5×5) supercells of surface unit cells. To accommodate the adsorption of contact ion pairs and solvent-separated ion pairs on graphite without undesirable periodic effects, a (6×6) supercell of the surface unit cell is utilized. For systems containing the graphite surface, we employ Gaussian smearing with a narrow width of 0.03 eV, while the first-order Methfessel-Paxton scheme [68] with a width of 0.2 eV is utilized for the cases with metal sodium surfaces.

4. Results and discussions

4.1. Adsorption characteristics of a NaOTF ion pair

We initiate our analysis by examining the adsorption characteristics of aggregated ions, the predominant ionic configuration in the NaOTF WiS electrolyte [43]. To this end, we start with a single NaOTF ion pair, which approximates 1:1 ion aggregation structures. According to Fig. 1, the examined ion pair demonstrates a tendency to adsorb onto both graphite and sodium surfaces, with the triflate anion adsorbing via its oxygen atoms. The calculated adsorption energies (see Fig. 1) reveal a stronger and more favorable adsorption of the ion pair on the sodium surface compared to graphite. This higher adsorption propensity on sodium likely arises from chemical interactions facilitated by the inherently high reactivity of sodium metal, a topic further elaborated in subsequent discussions. Consequently, while on graphite, the adsorbed ions maintain a distance of about 3 Å from the topmost layer (Fig. 1a), they approach the sodium surface closely (Fig. 1b and 1c). Specifically, on the bcc (100) sodium lattice, the NaOTF ion pair demonstrates a strong tendency for adsorption, characterized by a high adsorption energy of -2 eV, resulting in a short vertical distance of approximately 0.8 Å between the triflate oxygen and the topmost surface layer.

Figure 1 shows that the orientation of the anion in the adsorption complex is notably sensitive to the electrode material. On graphite, the S-C bond of the triflate anion tends to orient nearly

perpendicular to the electrode surface (Fig. 1a), suggesting the potential formation of a strongly ordered brush-like interfacial layer in direct contact with the surface. In contrast, the adsorbed anion adopts a tilted orientation on the sodium surface (Fig. 1, panels b and c). Furthermore, surface characteristics exhibit the potential to alter the anion-cation coordination configuration in the adsorption complex. Fig. 1b demonstrates a monodentate ion pair configuration on the hcp (0001) sodium surface, where the cation interacts with only one triflate oxygen. However, the coordination configuration shifts to a bidentate arrangement in the presence of both graphite and the bcc (100) sodium surface (Fig. 1, panels a and c), with the cation coordinating with two triflate oxygens. Considering the prevalent occurrence of monodentate configurations in bulk NaOTF WiS electrolyte (see Ref. [43]), this observation suggests that ion pairs involved in the aggregates may require less rearrangement to achieve their most stable configuration when adsorbed on the hcp (0001) sodium surface. However, we note that the resulting adsorption configuration may still be less stable than achievable on a bcc (100) sodium surface (see the adsorption energies presented in Fig. 1, panels b and c).

To capture the restructuring of surface atoms in the presence of adsorbed ions, we calculate the displacements of relaxing atoms in each surface model from their respective positions in the bare surface. This includes the topmost layer for all surface models, as well as the layer directly below it for graphite and the two layers below it for the sodium surfaces. The maximum displacements obtained for each layer are presented in Fig. 1, denoted by δ_1 for the topmost layer, and δ_2 and δ_3 for the subsequent layers. These results suggest a restructuring of the topmost layer atoms in the sodium metal surfaces, especially for the bcc (100) lattice, likely due to their strong chemical interactions with the adsorbate atoms. The positions of graphite atoms, however, remain almost unchanged after adsorption, indicating their weaker interactions with the ion pair, which are likely purely electrostatic, as discussed next.

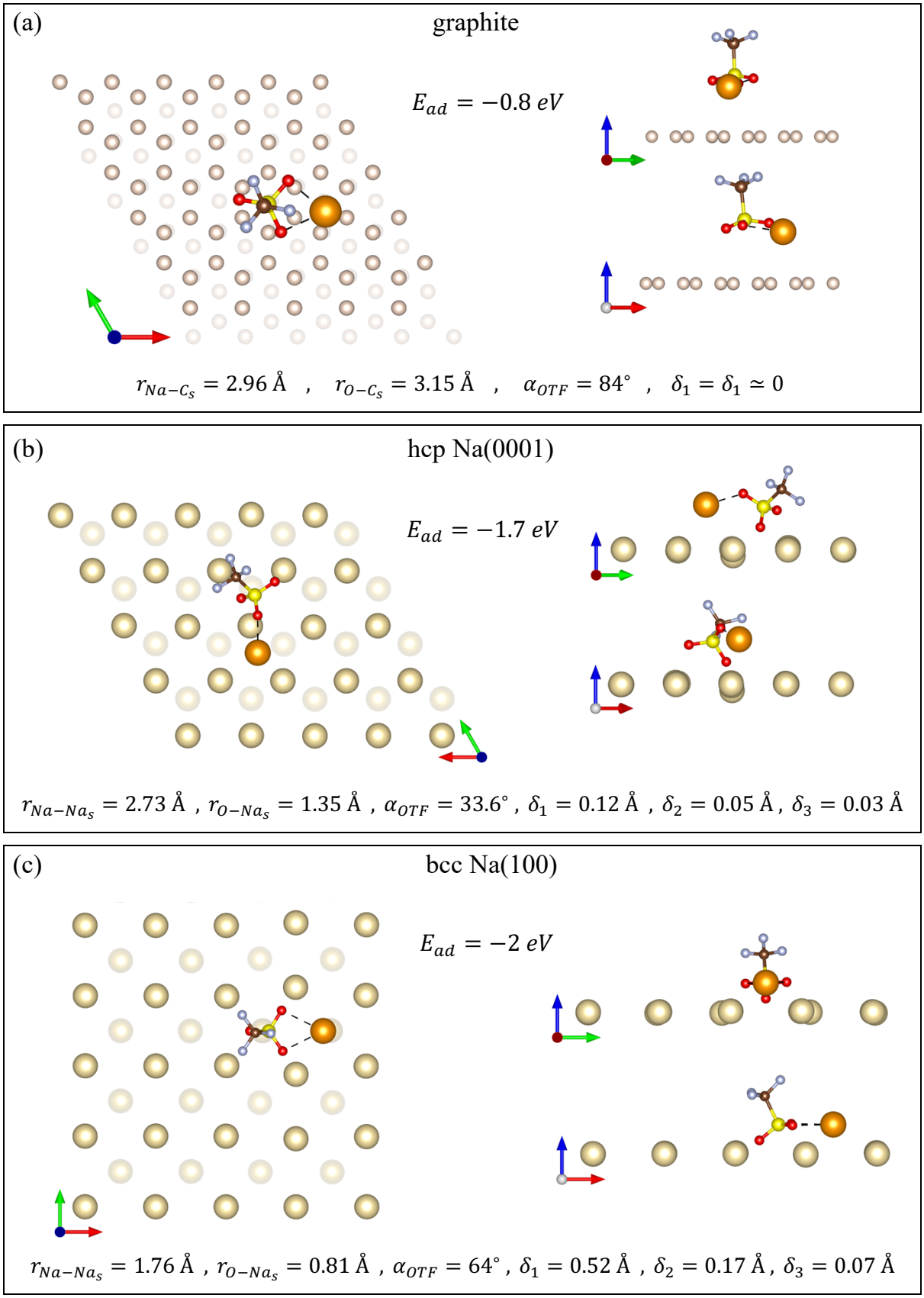

Figure 1. Top and side views of the adsorption structure of a NaOTF ion pair on the examined surface models: a) 3 layers of graphite, b) 4 layers of an hcp (0001) sodium lattice, and c) 4 layers of a bcc (100) sodium lattice. Each panel displays the corresponding adsorption energy, E_{ad},

obtained from Eq. 1, alongside key structural properties, including the vertical distance between the cation and the average position of atoms in the topmost surface layer, r_{Na-C_s} or r_{Na-Na_s}, the vertical distance between the closest anion oxygen to the surface and the average position of atoms in the topmost surface layer, r_{O-C_s} or r_{O-Na_s}, the angle between the S-C bond in the triflate anion and the surface plane, α_{OTF}, and the maximum atomic displacements in surface layers relative to the bare surface (δ_1 for the topmost layer, δ_2 for the second layer, and δ_3 for the third layer).

To gain deeper insights into the interfacial interactions, contour plots of charge rearrangement upon adsorption are presented in Fig. 2, illustrating the difference between the electron density of the adsorption complex and that of the isolated NaOTF ion pair and the bare surface. These plots demonstrate a region of enhanced charge density between the sodium cation and the surface atoms, suggesting some form of covalent interaction, alongside a region of reduced charge density between the triflate anion and the surface atoms. This implies the induction of a horizontal dipole moment in the interfacial region, opposite to that of the ion pair. The observed charge rearrangement is particularly pronounced on sodium surfaces, where regions of charge accumulation and depletion envelop the adsorbed ions (see Fig. 2, panels b and c). This suggests a notable charge transfer between the sodium surface and the adsorbed ions, potentially weakening the electrostatic attraction between cations and anions in the interfacial region. This could effectively reduce the interfacial resistance against cation diffusion, thereby enhancing ion conductivity within the resulting SEI. The contour plots also demonstrate small regions of enhanced charge density surrounding the oxygen atoms of the triflate anion, particularly for the anions adsorbed on the sodium metal surfaces (see Fig. 2, panels b and c). This suggests the formation of polar covalent bonds between these oxygen atoms and the highly electropositive sodium atoms at the electrode surface, giving rise to robust interactions between the electrode surface and the adsorbed anions. These interactions could play a pivotal role in promoting a stable SEI, a key factor in mitigating water decomposition on the electrode surface (see section 4.3 for more details).

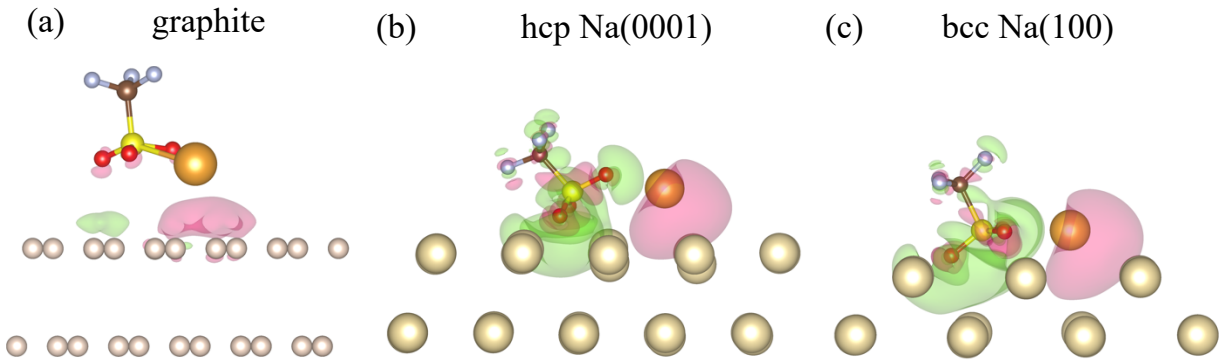

Figure 2. Charge rearrangements induced by the adsorption of a NaOTF ion pair on the examined surfaces: a) 3 layers of graphite, b) a 4-layer hcp (0001) sodium surface, and c) a 4-layer bcc (100) sodium surface. The figure displays the electron density difference using two isosurfaces (red:$+0.001\ e/\text{Å}^3$ and green:$-00.001\ e/\text{Å}^3$), showing the difference between the electron density of the adsorption complex and that of the isolated ion pair and the bare surface.

In the next step, we investigate the decomposition behavior of the triflate anion during the adsorption process. It is important to note that our analysis will now focus exclusively on graphite and the bcc (100) sodium surface. This decision is based on the observation that both the examined sodium surface models yield almost similar outcomes concerning the adsorption complex, with the bcc (100) lattice showing a higher adsorption energy. Our investigation considers potential decomposition products resulting from the breaking of the S-C bond (Fig. 3a), a single S-O bond (Fig. 3b), or a single C-F bond (Fig. 3c), as the initial decomposition reactions (see section 2 for technical details). Additionally, we explore scenarios involving breaking of multiple bonds, resulting in the decomposition of the anion into smaller products or its constituent atoms (see Fig. 3, panels d-h). The positive reaction energies obtained on the graphite surface ($\Delta E_{dec}^{S-C} = 2.46\ eV$, $\Delta E_{dec}^{S-O} = 3.13\ eV$, $\Delta E_{dec}^{C-F} = 2.64\ eV$) suggest that anion decomposition on this surface is not feasible, highlighting the inert nature of graphite. In contrast, during the adsorption process on the sodium metal surface, all considered decomposition scenarios are energetically favorable, as indicated by their negative reaction energies (Fig. 3). In this case, the breaking of the C-F bond exhibits the greatest energetic favorability as an initial decomposition reaction (Fig. 3c), followed by the breaking of the C-S

bond (Fig. 3a). The stability of the adsorption complex further increases with the simultaneous breaking of both the C-F and C-S bonds, yielding CF_2 and SO_3 products, as well as an individual fluorine atom that may closely associate with the sodium cation to form NaF (Fig. 3e). Subsequent decomposition of these products into atomic constituents provides the most stable adsorption structures, as illustrated in Fig. 3, panels g and h.

Comparing the decomposition behavior of the triflate anion on sodium versus graphite, we anticipate structural deviations in the interfacial layers directly forming on these electrodes. While the layer forming on the graphite surface is expected to primarily consist of sodium cations and intact triflate anions, with the triflate anions adsorbed in a perpendicular arrangement relative to the surface (as discussed in relation to Fig. 1), adsorption on the sodium metal surface is likely to yield a more disordered and heterogeneous layer, characterized by a notable presence of decomposed fluorine atoms and other potential anion decomposition products. Such characteristics could effectively contribute to the formation of a smooth layer covering the sodium surface, potentially mitigating dendrite growth, a critical challenge in sodium metal electrodes [69]. Although the disordered nature of the resulting interfacial layer may hinder ion transport within this region, potentially affecting the sodium intercalation process, the weakened cation-anion electrostatic attractions within this region (as discussed in relation to Fig. 2) can effectively contribute to reducing overall interfacial resistance, thereby facilitating sodium conductivity.

To monitor the restructuring of the sodium surface atoms in the presence of decomposition products, we calculate δ_1, δ_2, and δ_3 as outlined earlier in this section. Results indicate that anion decomposition extends lattice distortion to the inner layers of the surface, as evidenced by the increased δ_2 and δ_3 compared to when the adsorbed anion remains intact (see Figs. 1c and 3). This could be primarily attributed to the high affinity of decomposition products to approach the surface layer or penetrate the atomic structure of the electrode. Fig. 3 indicates

that unlike individual fluorine atoms and larger decomposition products such as SO_3, SO_2, CF_3, and CF_2, which predominantly adsorb at the surface or within the hollow positions at the topmost atomic layer (panels a and c-g), individual oxygen atoms may migrate into the bulk electrode and occupy interstitial sites within the lattice (panels b and h). This could potentially compromise the mechanical integrity of the electrode material and hinder ion diffusion within the electrode, thus affecting capacity and cycling stability of the battery. However, the potential association of detached oxygen atoms with the sodium cation, as suggested in Fig. 3, panels d and f, may prevent their unfavorable migration into the bulk electrode. To assess the likelihood of this scenario, additional ab initio molecular dynamics simulations are necessary.

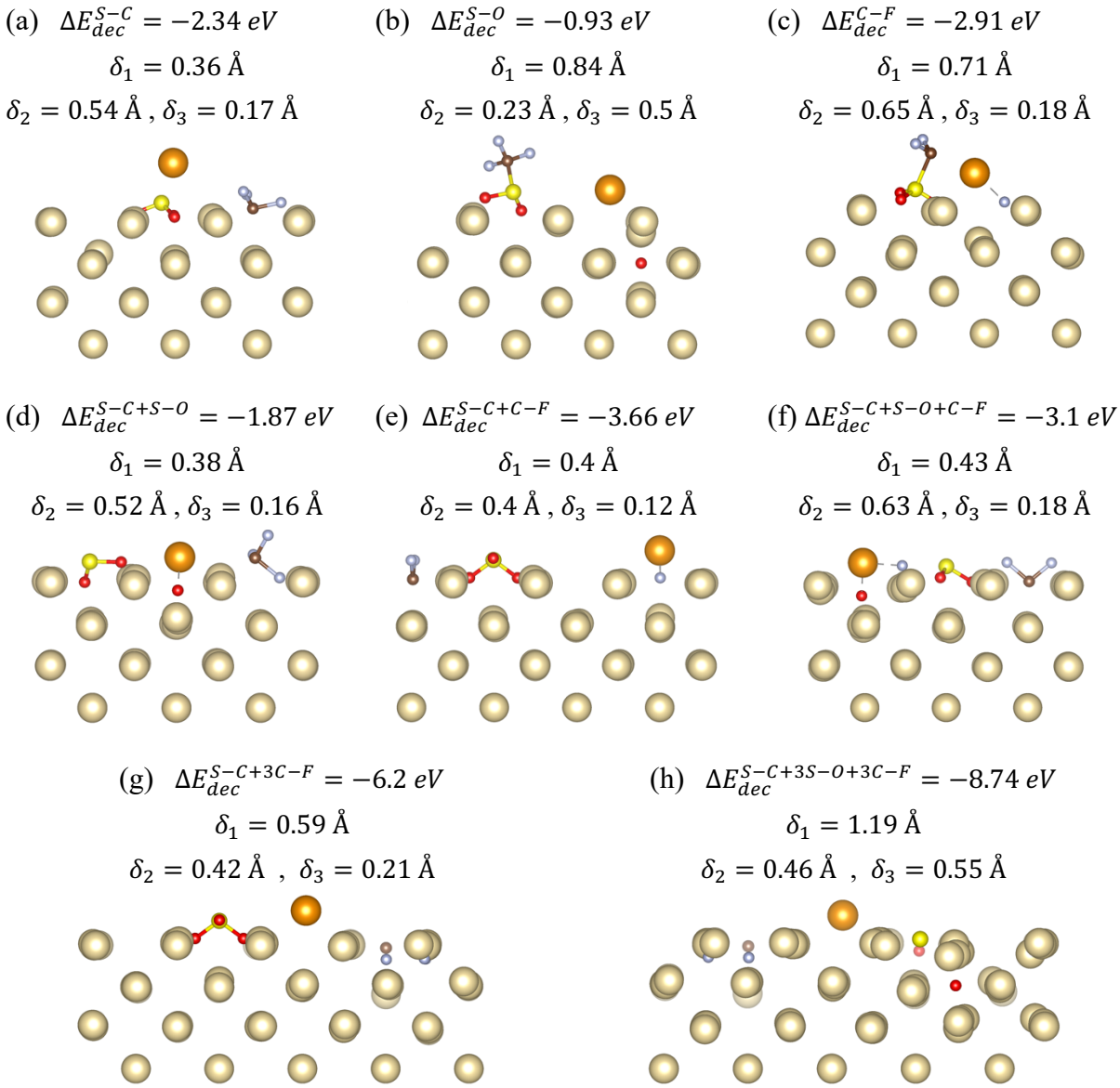

Figure 3. Potential adsorption structures of a NaOTF ion pair on a 4-layer bcc (100) sodium metal surface considering different anion decomposition scenarios. The decomposition products correspond to the breaking of: a) the S-C bond, b) one S-O bond, c) one C-F bond, d) the S-C plus one S-O bond, e) the S-C plus one C-F bond, f) the S-C plus one S-O plus one C-F bond, g) the S-C plus three C-F bonds, and h) the S-C plus three S-O plus three C-F bonds. Each panel displays the corresponding decomposition reaction energy (ΔE_{dec}) obtained from Eq. 2, and the maximum atomic displacements in surface layers relative to the bare surface (δ_1 for the topmost layer, δ_2 for the second layer, and δ_3 for the third layer).

4.2. Adsorption of Na_2OTF and $Na(OTF)_2$ structures

To explore additional potential sub-structures within the ion-rich domain of a NaOTF WiS electrolyte, we extend our analysis to the adsorption of Na_2OTF and $Na(OTF)_2$ aggregates on

the examined surfaces. While the resulting adsorption complexes closely resemble the structural properties of the adsorbed NaOTF ion pair in terms of the anion orientation relative to the surface (see Fig. 1, panels a and c, and Fig. 4), both the distance of the ions from the surface and the cation-anion coordination configuration exhibit dependency on the adsorbate structure. In particular, the cation in the adsorbed $Na(OTF)_2$ demonstrates a notably greater distance from the surface compared to that in the NaOTF and Na_2OTF adsorbates. Additionally, unlike other adsorption structures where the adsorbed cation is bidentately coordinated to the anion(s), the adsorbed Na_2OTF on the sodium surface exhibits two monodentate cation-anion configurations. Comparing the adsorption energies for the examined structures, the $Na(OTF)_2$ structure demonstrates the highest tendency to undergo adsorption, followed by the Na_2OTF and then the NaOTF structures (see Figs. 1 and 4). This suggests that larger aggregates, comprising multiple anions or cations, may have a greater propensity for adsorption onto solid surfaces compared to smaller aggregates or individual ions. This increased tendency could primarily stem from the increased number of atoms interacting with the surface, particularly when multiple anions are involved in the aggregate and come into contact with the surface. This underscores the importance of enhanced cation-anion coordination within WiS electrolytes for SEI formation, a concept also addressed in Refs. [43, 46]. Still, it is important to note that our analysis neglects additional mutual interactions in larger clusters, which could potentially influence the structure of the adsorption complexes and their adsorption energies.

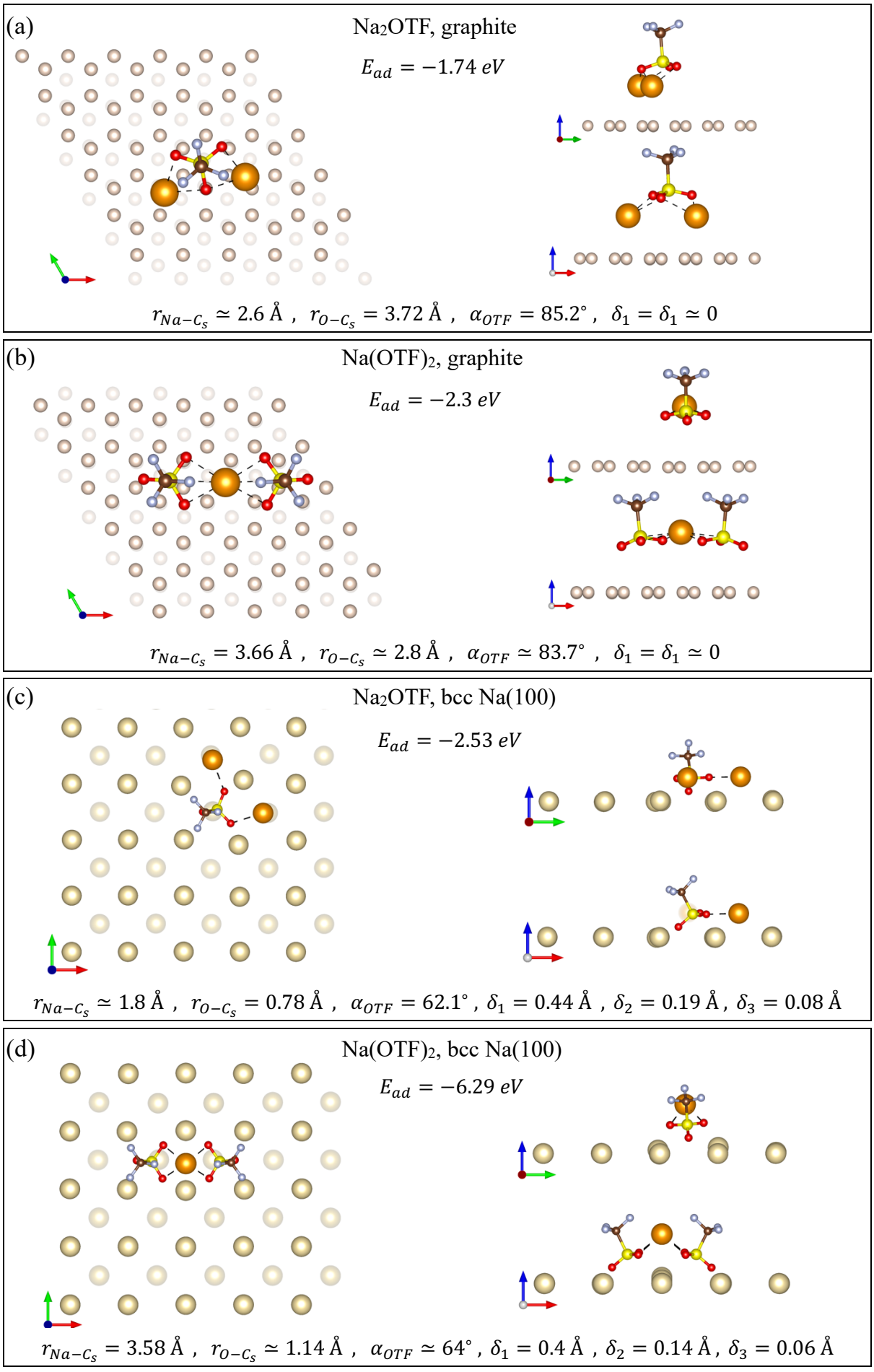

Figure 4. Top and side views of the adsorption structures of multi-ion complex models on the

examined surfaces: a) Na_2OTF on 3 layers of graphite, b) $Na(OTF)_2$ on 3 layers of graphite, c) Na_2OTF on a 4-layer bcc (100) sodium surface, and d) $Na(OTF)_2$ on a 4-layer bcc (100) sodium surface. Each panel displays the corresponding adsorption energy, E_{ad}, obtained from Eq. 1, alongside key structural properties: the vertical distance between the sodium cation and the average position of atoms in the topmost surface layer, r_{Na-C_s} or r_{Na-Na_s}, the vertical distance between the nearest oxygen atom of the triflate anion(s) to the surface and the average position of atoms in the topmost surface layer, r_{O-C_s} or r_{O-Na_s}, the angle between the S-C bond in the triflate anion and the surface plane, α_{OTF}, and the maximum atomic displacements in surface layers relative to the bare surface (δ_1 for the topmost layer, δ_2 for the second layer, and δ_3 for the third layer).

We now investigate the impact of cation-anion interactions within complex aggregate structures on the decomposition probability of triflate anions. To this end, following the procedure outlined in section 2, we exclusively explore the probability of breaking the C-F and S-C bonds, identified as the most probable initial decomposition reactions (see section 4.1). The positive reaction energies obtained in the presence of graphite ($\Delta E_{dec}^{S-C} = 0.78\ eV$ and $\Delta E_{dec}^{C-F} = 0.13\ eV$ for the Na_2OTF adsorbate, and $\Delta E_{dec}^{S-C} = 1.6\ eV$ and $\Delta E_{dec}^{C-F} = 1.88\ eV$ for the $Na(OTF)_2$ adsorbate) demonstrate a lack of propensity for anion decomposition during adsorption on the graphite surface, irrespective of the aggregate structure. In contrast, the anion shows a significant propensity for decomposition during adsorption onto the sodium surface, with the anions involved in $Na(OTF)_2$ and Na_2OTF aggregates demonstrating a higher tendency for decomposition compared to that observed for a NaOTF ion pair (see Fig. 3, panels a and c, and Fig. 5, panels a-d). This underscores the pronounced tendency for anion decomposition within the ion-rich domain of a NaOTF WiS electrolyte, where numerous anions and cations participate in aggregate formations, resulting in the prevalent formation of $Na(OTF)_2$, Na_2OTF, and analogous substructures.

Our results also demonstrate that when two triflates are in contact with the same cation, forming a $Na(OTF)_2$ substructure, the breaking of the S-C bond in one anion enhances the probability of a similar bond breaking in the second anion, as indicated by $\left|\Delta E_{dec}^{2S-C}\right| > 2\left|\Delta E_{dec}^{S-C}\right|$. Conversely, when one anion loses a fluorine atom, the second one shows a decreased, but still

significant, tendency to undergo fluorine loss, as evidenced by $\left|\Delta E_{dec}^{2C-F}\right| < 2\left|\Delta E_{dec}^{C-F}\right|$. This behavior indicates that the presence of multiple anions in the aggregate substructures influences the energetics of bond breaking in a non-linear manner.

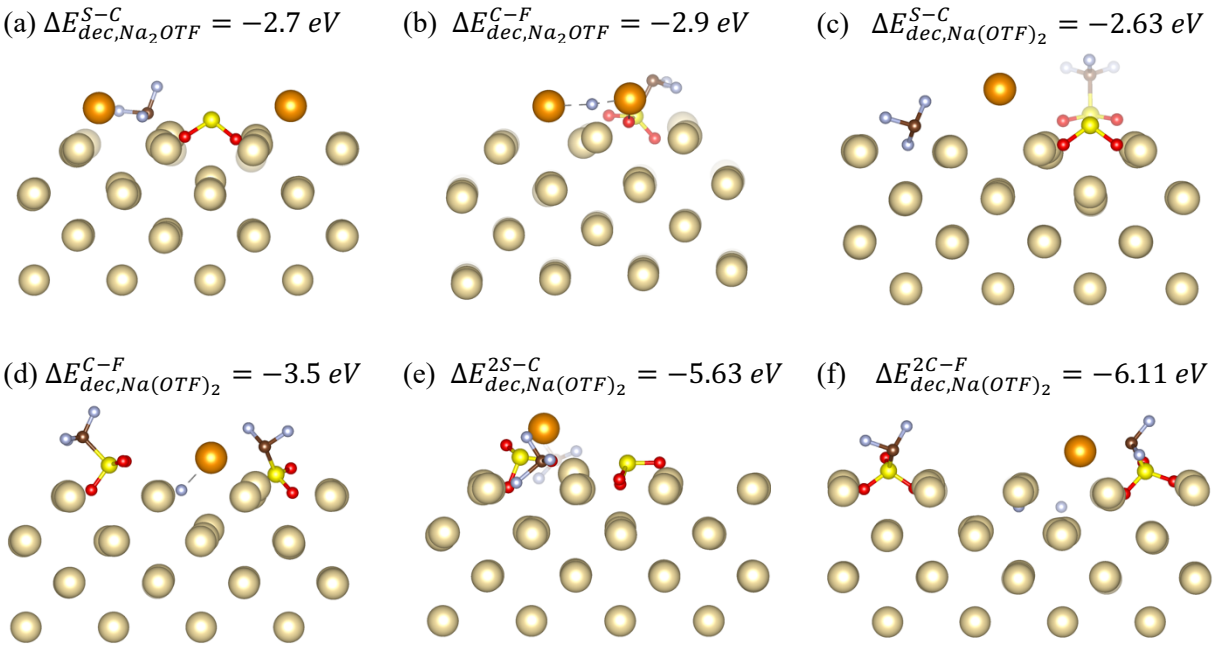

Figure 5. Structures of potential decomposition products of triflate anion(s) during adsorption of Na_2OTF and $Na(OTF)_2$ aggregates on a bcc (100) sodium surface. These structures represent the breaking of: a) the S-C bond in Na_2OTF, b) one C-F bond in Na_2OTF, c) one S-C bond in $Na(OTF)_2$, d) one C-F bond in $Na(OTF)_2$, e) both S-C bonds in $Na(OTF)_2$, and f) two C-F bonds from different anions in $Na(OTF)_2$. Each panel displays the corresponding decomposition reaction energy, ΔE_{dec}, obtained from Eq. 2.

4.3. Approximation models for the adsorption of solvated ion pairs

To better understand the initial stages of SEI formation on the examined surface models, it is important to consider the potential presence of water within the interfacial region, as it can significantly affect the stability and arrangement of the adsorbed ion species. To address this, we conduct new simulations in the presence of water molecules. In our analysis, we assume that the salt concentration in the bulk electrolyte is sufficiently high to exclude the presence of free water molecules and free ions, as expected in the WiS regime [43]. Consequently, only water molecules within the solvation shells of contact ion pairs and solvent-separated ion pairs can approach the electrode surface and contribute to SEI formation. For the NaOTF WiS

electrolyte, this assumption corresponds to a salt concentration of approximately $9.25\,m$ or higher, as determined in our previous research [43].

To ensure the inclusion of sufficient water molecules for modeling contact and solvent-separated ion pair structures, we conduct a preliminary molecular dynamics analysis. This involves increasing the number of water molecules surrounding a single NaOTF ion pair within a large simulation box ($45 \times 45 \times 45$ Å^3) and examining ion-ion and water-ion configurations to achieve the desired contact or solvent-separated arrangements. For this purpose, we employ the OPLS force field [70] for ions and the SPC/E model [71] for water. Based on this analysis, we develop contact and solvent-separated ion pair models comprising 12 and 24 water molecules, respectively, which are then used in our DFT calculations. While our consistent use of DFT modeling for various adsorption scenarios in the presence of water allows for comparisons of energetic favorability among the resulting adsorption structures, it is important to acknowledge the limitations of our DFT model. Firstly, this model does not fully capture the complexities of ion desolvation during the adsorption process, as it neglects temperature effects, dynamic processes, and certain aspects of mutual interactions between the solvated ions and their neighboring electrolyte components. Secondly, the adsorption energies are determined with respect to ion pairs and their surrounding water molecules in the gas phase, which may introduce potential errors when applied to the liquid electrolyte environment. Therefore, subsequent ab initio molecular dynamics simulations are necessary for a more precise analysis of the SEI formation in the presence of solvation shells.

By yielding negative adsorption energies, our DFT calculations suggest the potential presence of fully solvated contact and solvent-separated ion pairs in close proximity to the graphite surface (see Fig. 6, panels a and c). However, the proximity of both these structures to the surface will likely result in the partial loss of their solvation shells and their direct adsorption onto the graphite surface, thus achieving higher energetic stability, as evidenced by $\Delta E_{des} < 0$ (see Fig. 6, panels b and d). This suggests a low probability of finding water within the first

layer directly covering the surface, though some water molecules might be present in subsequent layers, participating in the solvation shells of the adsorbed ions. Nevertheless, the interfacial region is predicted to primarily consist of large aggregates, which could enhance overall energetic stability during their adsorption onto the graphite surface, as evidenced by the large adsorption energies of Na_2OTF and $NaOTF_2$ structures (see Fig. 4).

In the presence of the sodium surface, our DFT calculations yield positive adsorption energies for contact and solvent-separated ion pair structures (Fig. 6, panels e and g), suggesting their minimal presence in close proximity to the surface. Although partial desolvation enhances the stability of the adsorbed structures, as reflected in $\Delta E_{des} < 0$ (Fig. 6, panels f and h), the positive adsorption energies obtained for the fully solvated structures still act as a barrier against their approach to the surface and subsequent desolvation. Consequently, ions are anticipated to form the vast majority of adsorbed species on the sodium surface, with water rarely present within the interfacial region. The absence of water in this region could significantly contribute to expanding the electrochemical stability window by inhibiting water-surface interactions, thus preventing water reduction on the electrode surface.

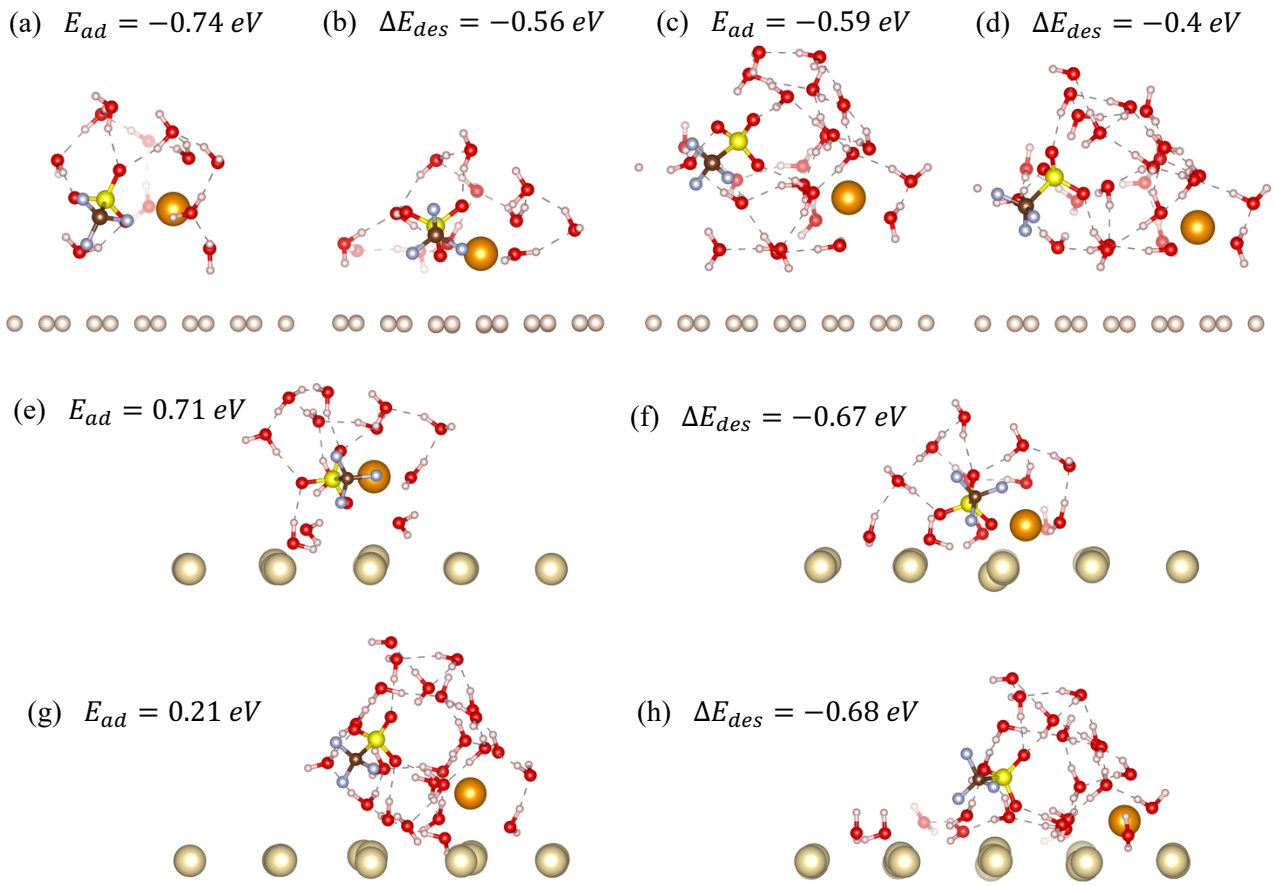

Figure 6. Structures of contact and solvent-separated ion pair models in proximity to the examined surfaces: a-d) 3 layers of graphite, and e-h) a 4-layer bcc (100) sodium surface. The panels show fully solvated contact (a and e) and solvent-separated (c and g) ion pair structures, as well as partly desolvated contact (b and f) and solvent-separated (d and h) ion pair structures. For the fully solvated adsorbates, the corresponding panels display the adsorption energies, E_{ad}, obtained from Eq. 1, and for the partly desolvated adsorbates, the panels show the desolvation energies, ΔE_{des}, approximated from Eq. 3.

While our findings suggest minimal water presence near the graphite and sodium metal electrodes, it remains imperative to investigate the probability of water decomposition on these electrodes, as it may significantly impact the electrochemical stability window. To achieve this, we examine the energetic favorability of water reduction (see Eq. 4) on the electrode surface by selectively breaking two O-H bonds from two adjacent water molecules (see section 2 for more details). Our investigations exclusively consider the water molecules within the partly desolvated contact and solvent-separated ion pairs directly adsorbed onto the surface, as they represent the most stable water-containing adsorption complexes before water decomposition

(see Fig. 6). Positive reaction energies obtained from Eq. 2 in the presence of graphite ($\Delta E_{dec} = 3.6\ eV$) indicate the unlikelihood of water reduction at the interface between the examined WiS electrolyte and inert graphitic electrodes, aligning with the stability objectives in WiS electrolyte design. In contrast, calculations in the presence of the highly reactive sodium metal surface yield relatively large negative decomposition energies (see Fig. 7), indicating a strong tendency for water reduction. Thus, if water molecules reach the layer covering the sodium surface, they are likely to undergo reduction, leading to the formation of sodium hydroxide and hydrogen gas (see Fig. 7). This process can ultimately compromise the electrochemical stability and impact battery performance. Therefore, it is crucial to achieve a water-lacking SEI on the sodium metal electrode when using a WiS electrolyte. Based on the insights derived from our present investigation and the findings of our previous study [43], this objective can be effectively pursued by increasing the salt concentration to a sufficiently high level where both free water molecules and free ions are absent in the bulk electrolyte. In such a system, water can only access the electrode surface as part of solvation shells around contact and solvent-separated ion pairs. However, these structures exhibit minimal tendency to approach the sodium metal surface (see Fig. 6, panels e and g), thereby effectively reducing the probability of water decomposition on the sodium metal electrode.

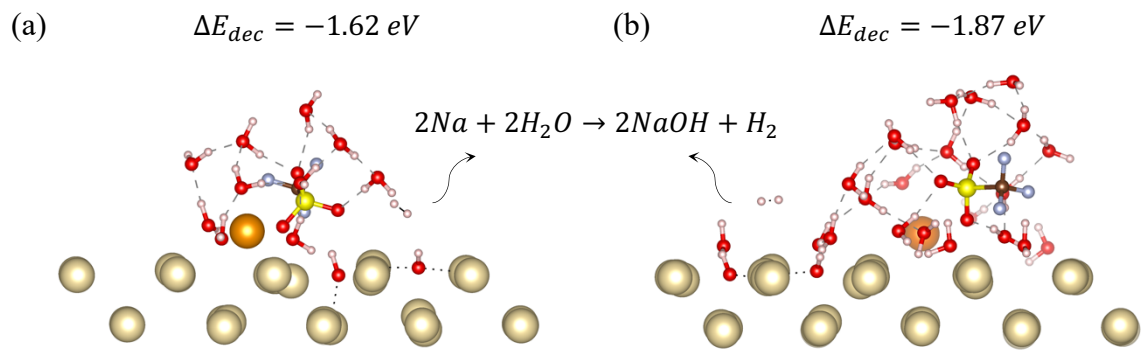

Figure 7. Exemplary water decomposition products resulting from the reduction of water molecules approached a 4-layer bcc (100) sodium surface as part of adsorbed contact (panel a) and solvent-separated (panel b) ion pair structures. Each panel displays the corresponding decomposition reaction energy, ΔE_{dec}, obtained from Eq. 2 with respect to the adsorption complexes containing intact water molecules.

Conclusion

Density functional theory (DFT) calculations, coupled with an ionic relaxation algorithm, are employed to explore the initial stages of solid-electrolyte interphase (SEI) formation in a sodium triflate (NaOTF) water-in-salt (WiS) electrolyte, a critical factor in ensuring electrochemical stability. The study focuses on two distinct electrode materials: graphite, commonly used as an inert electrode in sodium-ion batteries, and sodium metal, representing a highly reactive solid phase, either as a bulk electrode or a thin film grown on the electrode surface. In both scenarios, triflate anions are observed to adsorb onto the solid surface via their oxygen atoms, with multi-ion aggregates exhibiting a stronger adsorption tendency. This highlights the importance of enhanced cation-anion coordination within WiS electrolytes in promoting a stable SEI. While both the graphite and sodium metal electrodes show potential for forming this protective layer and ensuring sufficient electrochemical stability in the presence of a NaOTF WiS electrolyte, the mechanism underlying SEI formation and the structure of the adsorbed complexes covering the electrode surface are found to depend significantly on surface characteristics.

On graphite, the adsorption process may lead to the formation of an interfacial layer comprising intact anions, cations, and water molecules, all maintaining a vertical distance of at least 2.9 Å from the surface layer. This suggests a purely electrostatic nature for the corresponding solid-electrolyte interactions, which could potentially compromise SEI stability in the absence of robust chemical interactions. However, the presence of large aggregates within the WiS electrolyte can improve the stability of the SEI by involving multiple anions in the SEI formation. The corresponding triflate anions tend to adsorb onto the surface with their C-S bonds nearly perpendicular to the surface, potentially forming a brush-like interfacial structure. This configuration has the potential to reduce interfacial resistance to ion conductivity, thus facilitating the cation intercalation process. Ultimately, it can lead to more efficient charge and discharge processes, thereby enhancing overall battery performance. On the other hand, the

potential presence of water molecules within the interfacial layer poses a risk of water decomposition that can compromise the electrolyte stability and reduce battery performance. However, we note that the inert carbon atoms within the graphite surface lack the energy required for initiating water decomposition and subsequent reduction reactions. Therefore, from both the electrochemical stability and ion conductivity perspectives, graphite, and likely other carbon-based electrodes, could be considered as potential candidates for use in batteries featuring a NaOTF WiS electrolyte.

Unlike on graphite, triflate anions adsorbed on the sodium metal exhibit a strong tendency to approach the surface closely and form robust covalent bonds with the surface atoms via their oxygen atoms. These strong interfacial interactions not only enhance the stability of the resulting SEI compared to that on graphite, but also alter the arrangement of the adsorbed anions, resulting in tilted configurations. Additionally, the inherently high reactivity of the sodium surface provides an energetically favorable environment for anion decomposition during the adsorption process, resulting in an extensive formation of smaller decomposition products that strongly interact with the surface atoms. These decomposition products, which may include SO_3, CF_3, and CF_2 groups, as well as atomic constituents like F, C, and O, tend to preferentially adsorb in hollow positions at the surface, leading to the formation of a smooth layer covering the electrode surface.

Despite the potential formation of a strongly stable SEI on the sodium metal surface, even minimal penetration of water molecules into the interfacial region can pose a significant risk of water decomposition on this highly electropositive electrode. Hence, in the absence of free water molecules, we examined the potential presence of water within the interfacial layer as part of ion solvation shells. Our simulations indicate that the solvated ion structures exhibit energetic unfavorability when approaching the sodium surface. This strongly suggests an absence of water in close proximity to the electrode surface, effectively ensuring electrochemical stability. Additionally, our findings indicate a notable charge transfer between

the sodium surface and the adsorbed cations and anions, leading to a weakening of the electrostatic attraction between cations and anions in the interfacial region. This could potentially enhance the cation intercalation process, thereby ensuring efficient charge and discharge cycles. Consequently, despite the challenges associated with their highly reactive nature, sodium metal electrodes hold promise for delivering desirable characteristics when coupled with an NaOTF WiS electrolyte.

Associated Content

Supporting Information

Additional details on the initial DFT calculations (PDF)

Data Availability Statement

The data underlying this study, including sample input and output files for the DFT calculations, are openly available in Zenodo at https://doi.org/10.5281/zenodo.13903623.

ACKNOWLEDGMENTS

This work was funded by the Deutsche Forschungsgemeinschaft (DFG, German Research Foundation) under Project ID 390874152 (POLiS Cluster of Excellence). Computer time provided by the state of Baden-Württemberg through bwHPC and the German Research Foundation (DFG) under grant no INST 40/575-1 FUGG (JUSTUS 2 cluster) is gratefully acknowledged. This work contributes to the research performed at the Center for Electrochemical Energy Storage Ulm-Karlsruhe (CELEST).

References

(1) Tarascon, J. M.; Armand, M. Issues and challenges facing rechargeable lithium batteries. *Nature* **2001**, *414* (6861), 359-367. DOI: 10.1038/35104644.
(2) Nitta, N.; Wu, F.; Lee, J. T.; Yushin, G. Li-ion battery materials: present and future. *Materials Today* **2015**, *18* (5), 252-264. DOI: https://doi.org/10.1016/j.mattod.2014.10.040.
(3) Wanger, T. C. The Lithium future—resources, recycling, and the environment. *Conservation Letters* **2011**, *4* (3), 202-206. DOI: https://doi.org/10.1111/j.1755-263X.2011.00166.x.
(4) Janek, J.; Zeier, W. G. A solid future for battery development. *Nature Energy* **2016**, *1* (9), 16141. DOI: 10.1038/nenergy.2016.141.

(5) Kalhoff, J.; Eshetu, G. G.; Bresser, D.; Passerini, S. Safer Electrolytes for Lithium-Ion Batteries: State of the Art and Perspectives. *ChemSusChem* **2015**, *8* (13), 2154-2175. DOI: https://doi.org/10.1002/cssc.201500284 (acccessed 2024/08/06).
(6) Elia, G. A.; Marquardt, K.; Hoeppner, K.; Fantini, S.; Lin, R.; Knipping, E.; Peters, W.; Drillet, J.-F.; Passerini, S.; Hahn, R. An Overview and Future Perspectives of Aluminum Batteries. *Advanced Materials* **2016**, *28* (35), 7564-7579. DOI: https://doi.org/10.1002/adma.201601357.
(7) Vera, M. L.; Torres, W. R.; Galli, C. I.; Chagnes, A.; Flexer, V. Environmental impact of direct lithium extraction from brines. *Nature Reviews Earth & Environment* **2023**, *4* (3), 149-165. DOI: 10.1038/s43017-022-00387-5.
(8) Zeng, X.; Li, J.; Singh, N. Recycling of Spent Lithium-Ion Battery: A Critical Review. *Critical Reviews in Environmental Science and Technology* **2014**, *44* (10), 1129-1165. DOI: 10.1080/10643389.2013.763578.
(9) Ponrouch, A.; Monti, D.; Boschin, A.; Steen, B.; Johansson, P.; Palacín, M. R. Non-aqueous electrolytes for sodium-ion batteries. *Journal of Materials Chemistry A* **2015**, *3* (1), 22-42, 10.1039/C4TA04428B. DOI: 10.1039/C4TA04428B.
(10) Hwang, J. Y.; Myung, S. T.; Sun, Y. K. Sodium-ion batteries: present and future. *Chem Soc Rev* **2017**, *46* (12), 3529-3614. DOI: 10.1039/c6cs00776g From NLM.
(11) Hasa, I.; Tapia-Ruiz, N.; Galceran, M. Editorial: Sodium-ion batteries: From materials discovery and understanding to cell development. *Frontiers in Energy Research* **2022**, *10*, Editorial. DOI: 10.3389/fenrg.2022.1076764.
(12) Kumar Prajapati, A.; Bhatnagar, A. A review on anode materials for lithium/sodium-ion batteries. *Journal of Energy Chemistry* **2023**, *83*, 509-540. DOI: https://doi.org/10.1016/j.jechem.2023.04.043.
(13) Wan, Y.; Huang, B.; Liu, W.; Chao, D.; Wang, Y.; Li, W. Fast-Charging Anode Materials for Sodium-Ion Batteries. *Advanced Materials n/a* (n/a), 2404574. DOI: https://doi.org/10.1002/adma.202404574.
(14) Wu, C.; Yang, Y.; Zhang, Y.; Xu, H.; He, X.; Wu, X.; Chou, S. Hard carbon for sodium-ion batteries: progress, strategies and future perspective. *Chemical Science* **2024**, *15* (17), 6244-6268, 10.1039/D4SC00734D. DOI: 10.1039/D4SC00734D.
(15) Fichtner, M. Recent Research and Progress in Batteries for Electric Vehicles. *Batteries & Supercaps* **2022**, *5* (2), e202100224. DOI: https://doi.org/10.1002/batt.202100224.
(16) Vaalma, C.; Buchholz, D.; Weil, M.; Passerini, S. A cost and resource analysis of sodium-ion batteries. *Nature Reviews Materials* **2018**, *3* (4), 18013. DOI: 10.1038/natrevmats.2018.13.
(17) Choi, J. W.; Aurbach, D. Promise and reality of post-lithium-ion batteries with high energy densities. *Nature Reviews Materials* **2016**, *1* (4), 16013. DOI: 10.1038/natrevmats.2016.13.
(18) Lu, W.; Wang, Z.; Zhong, S. Sodium-ion battery technology: Advanced anodes, cathodes and electrolytes. *Journal of Physics: Conference Series* **2021**, *2109* (1), 012004. DOI: 10.1088/1742-6596/2109/1/012004.
(19) Alptekin, T.-R. N. A. A.; Barker, H. A. M. A. H. J. Boston R. Brant WR Brittain JM Chen YJ Phys. *Energy* **2021**, *3*, 031503.
(20) Hasa, I.; Sathiya, M.; Saurel, D.; Adelhelm, P.; Koposov, A., Y.; Masquelier, C.; Croguennec, L.; Casas-Cabanas, M. Challenges of today for Na-based batteries of the future: From materials to cell metrics. *Journal of Power Sources* **2021**, *482*, 228872 (228827 p.). DOI: 10.1016/j.jpowsour.2020.228872 Univ-nantes
(21) Wang, L.; Song, J.; Qiao, R.; Wray, L. A.; Hossain, M. A.; Chuang, Y.-D.; Yang, W.; Lu, Y.; Evans, D.; Lee, J.-J. Rhombohedral Prussian white as cathode for rechargeable sodium-ion batteries. *Journal of the American Chemical Society* **2015**, *137* (7), 2548-2554.
(22) Zuo, W.; Innocenti, A.; Zarrabeitia, M.; Bresser, D.; Yang, Y.; Passerini, S. Layered oxide cathodes for sodium-ion batteries: storage mechanism, electrochemistry, and techno-economics. *Accounts of Chemical Research* **2023**, *56* (3), 284-296.

(23) Kubota, K.; Komaba, S. Review—Practical Issues and Future Perspective for Na-Ion Batteries. *Journal of The Electrochemical Society* **2015**, *162* (14), A2538. DOI: 10.1149/2.0151514jes.
(24) Schafzahl, L.; Hanzu, I.; Wilkening, M.; Freunberger, S. A. An Electrolyte for Reversible Cycling of Sodium Metal and Intercalation Compounds. *ChemSusChem* **2017**, *10* (2), 401-408. DOI: https://doi.org/10.1002/cssc.201601222.
(25) Komaba, S.; Ishikawa, T.; Yabuuchi, N.; Murata, W.; Ito, A.; Ohsawa, Y. Fluorinated Ethylene Carbonate as Electrolyte Additive for Rechargeable Na Batteries. *ACS Applied Materials & Interfaces* **2011**, *3* (11), 4165-4168. DOI: 10.1021/am200973k.
(26) Lee, Y.; Lee, J.; Kim, H.; Kang, K.; Choi, N.-S. Highly stable linear carbonate-containing electrolytes with fluoroethylene carbonate for high-performance cathodes in sodium-ion batteries. *Journal of Power Sources* **2016**, *320*, 49-58. DOI: https://doi.org/10.1016/j.jpowsour.2016.04.070.
(27) Dugas, R.; Ponrouch, A.; Gachot, G.; David, R.; Palacin, M. R.; Tarascon, J. M. Na Reactivity toward Carbonate-Based Electrolytes: The Effect of FEC as Additive. *Journal of The Electrochemical Society* **2016**, *163* (10), A2333. DOI: 10.1149/2.0981610jes.
(28) Sun, Y.; Shi, P.; Xiang, H.; Liang, X.; Yu, Y. High-Safety Nonaqueous Electrolytes and Interphases for Sodium-Ion Batteries. *Small* **2019**, *15* (14), 1805479. DOI: https://doi.org/10.1002/smll.201805479 (acccessed 2024/08/08).
(29) Welton, T. Room-Temperature Ionic Liquids. Solvents for Synthesis and Catalysis. *Chemical Reviews* **1999**, *99* (8), 2071-2084. DOI: 10.1021/cr980032t.
(30) Armand, M.; Endres, F.; MacFarlane, D. R.; Ohno, H.; Scrosati, B. Ionic-liquid materials for the electrochemical challenges of the future. *Nature Materials* **2009**, *8* (8), 621-629. DOI: 10.1038/nmat2448.
(31) Giffin, G. A. Ionic liquid-based electrolytes for "beyond lithium" battery technologies. *Journal of Materials Chemistry A* **2016**, *4* (35), 13378-13389, 10.1039/C6TA05260F. DOI: 10.1039/C6TA05260F.
(32) Vogl, T.; Vaalma, C.; Buchholz, D.; Secchiaroli, M.; Marassi, R.; Passerini, S.; Balducci, A. The use of protic ionic liquids with cathodes for sodium-ion batteries. *Journal of Materials Chemistry A* **2016**, *4* (27), 10472-10478, 10.1039/C6TA02277D. DOI: 10.1039/C6TA02277D.
(33) Sun, H.; Zhu, G.; Xu, X.; Liao, M.; Li, Y.-Y.; Angell, M.; Gu, M.; Zhu, Y.; Hung, W. H.; Li, J. A safe and non-flammable sodium metal battery based on an ionic liquid electrolyte. *Nature communications* **2019**, *10* (1), 3302.
(34) Sirengo, K.; Babu, A.; Brennan, B.; Pillai, S. C. Ionic liquid electrolytes for sodium-ion batteries to control thermal runaway. *Journal of Energy Chemistry* **2023**, *81*, 321-338.
(35) Chagas, L. G.; Jeong, S.; Hasa, I.; Passerini, S. Ionic liquid-based electrolytes for sodium-ion batteries: tuning properties to enhance the electrochemical performance of manganese-based layered oxide cathode. *ACS applied materials & interfaces* **2019**, *11* (25), 22278-22289.
(36) Hagiwara, R.; Matsumoto, K.; Hwang, J.; Nohira, T. Sodium ion batteries using ionic liquids as electrolytes. *The Chemical Record* **2019**, *19* (4), 758-770.
(37) Monti, D.; Jónsson, E.; Palacin, M. R.; Johansson, P. Ionic liquid based electrolytes for sodium-ion batteries: Na+ solvation and ionic conductivity. *Journal of Power Sources* **2014**, *245*, 630-636.
(38) Shamsuri, A.; Abdullah, D. Ionic liquids: Preparations and limitations. *MAKARA, SAINS* **2010**, *14*, 101-106. DOI: 10.7454/mss.v14i2.677.
(39) Vo, T. D.; Nguyen, H. V.; Nguyen, Q. D.; Phung, Q.; Tran, V. M.; Le, P. L. M. Carbonate Solvents and Ionic Liquid Mixtures as an Electrolyte to Improve Cell Safety in Sodium-Ion Batteries. *Journal of Chemistry* **2019**, *2019* (1), 7980204. DOI: https://doi.org/10.1155/2019/7980204.
(40) Suo, L.; Borodin, O.; Gao, T.; Olguin, M.; Ho, J.; Fan, X.; Luo, C.; Wang, C.; Xu, K. "Water-in-salt" electrolyte enables high-voltage aqueous lithium-ion chemistries. *Science* **2015**, *350* (6263), 938-943. DOI: doi:10.1126/science.aab1595.

(41) Suo, L.; Borodin, O.; Wang, Y.; Rong, X.; Sun, W.; Fan, X.; Xu, S.; Schroeder, M. A.; Cresce, A. V.; Wang, F.; et al. "Water-in-Salt" Electrolyte Makes Aqueous Sodium-Ion Battery Safe, Green, and Long-Lasting. *Advanced Energy Materials* **2017**, *7* (21), 1701189. DOI: https://doi.org/10.1002/aenm.201701189.
(42) Suo, L.; Borodin, O.; Sun, W.; Fan, X.; Yang, C.; Wang, F.; Gao, T.; Ma, Z.; Schroeder, M.; von Cresce, A.; et al. Advanced High-Voltage Aqueous Lithium-Ion Battery Enabled by "Water-in-Bisalt" Electrolyte. *Angewandte Chemie International Edition* **2016**, *55* (25), 7136-7141. DOI: https://doi.org/10.1002/anie.201602397.
(43) Rezaei, M.; Sakong, S.; Groß, A. Sodium Triflate Water-in-Salt Electrolytes in Advanced Battery Applications: A First-Principles-Based Molecular Dynamics Study. *ACS Applied Materials & Interfaces* **2024**. DOI: 10.1021/acsami.4c01449.
(44) Zhang, T.; Li, D.; Tao, Z.; Chen, J. Understanding electrode materials of rechargeable lithium batteries via DFT calculations. *Progress in Natural Science: Materials International* **2013**, *23* (3), 256-272. DOI: https://doi.org/10.1016/j.pnsc.2013.04.005.
(45) Rezaei, M.; Sakong, S.; Groß, A. Molecular Modeling of Water-in-Salt Electrolytes: A Comprehensive Analysis of Polarization Effects and Force Field Parameters in Molecular Dynamics Simulations. *Journal of Chemical Theory and Computation* **2023**, *19* (17), 5712-5730. DOI: 10.1021/acs.jctc.3c00171.
(46) Han, J.; Mariani, A.; Passerini, S.; Varzi, A. A perspective on the role of anions in highly concentrated aqueous electrolytes. *Energy & Environmental Science* **2023**, *16* (4), 1480-1501, 10.1039/D2EE03682G. DOI: 10.1039/D2EE03682G.
(47) von Kolzenberg, L.; Latz, A.; Horstmann, B. Solid–Electrolyte Interphase During Battery Cycling: Theory of Growth Regimes. *ChemSusChem* **2020**, *13* (15), 3901-3910. DOI: https://doi.org/10.1002/cssc.202000867.
(48) Song, J.; Xiao, B.; Lin, Y.; Xu, K.; Li, X. Interphases in Sodium-Ion Batteries. *Advanced Energy Materials* **2018**, *8* (17), 1703082. DOI: https://doi.org/10.1002/aenm.201703082.
(49) Hosokawa, T.; Matsumoto, K.; Nohira, T.; Hagiwara, R.; Fukunaga, A.; Sakai, S.; Nitta, K. Stability of Ionic Liquids against Sodium Metal: A Comparative Study of 1-Ethyl-3-methylimidazolium Ionic Liquids with Bis(fluorosulfonyl)amide and Bis(trifluoromethylsulfonyl)amide. *The Journal of Physical Chemistry C* **2016**, *120* (18), 9628-9636. DOI: 10.1021/acs.jpcc.6b02061.
(50) Forsyth, M.; Hilder, M.; Zhang, Y.; Chen, F.; Carre, L.; Rakov, D. A.; Armand, M.; Macfarlane, D. R.; Pozo-Gonzalo, C.; Howlett, P. C. Tuning Sodium Interfacial Chemistry with Mixed-Anion Ionic Liquid Electrolytes. *ACS Applied Materials & Interfaces* **2019**, *11* (46), 43093-43106. DOI: 10.1021/acsami.9b12913.
(51) Ferdousi, S. A.; O'Dell, L. A.; Hilder, M.; Barlow, A. J.; Armand, M.; Forsyth, M.; Howlett, P. C. SEI Formation on Sodium Metal Electrodes in Superconcentrated Ionic Liquid Electrolytes and the Effect of Additive Water. *ACS Applied Materials & Interfaces* **2021**, *13* (4), 5706-5720. DOI: 10.1021/acsami.0c18119.
(52) Forster-Tonigold, K.; Buchner, F.; Groß, A.; Behm, R. J. Reactive Interactions between the Ionic Liquid BMP-TFSI and a Na Surface. *Batteries & Supercaps* **2023**, *6* (12), e202300336. DOI: https://doi.org/10.1002/batt.202300336.
(53) Stottmeister, D.; Groß, A. Toward the Formation of the Solid Electrolyte Interphase on Alkaline Metal Anodes: Ab Initio Simulations. *Batteries & Supercaps* **2023**, *6* (8), e202300156. DOI: https://doi.org/10.1002/batt.202300156.
(54) Buchner, F.; Forster-Tonigold, K.; Bolter, T.; Rampf, A.; Klein, J.; Groß, A.; Behm, R. J. Interaction of Mg with the ionic liquid 1-butyl-1-methylpyrrolidinium bis(trifluoromethylsulfonyl)imide—An experimental and computational model study of the electrode–electrolyte interface in post-lithium batteries. *Journal of Vacuum Science & Technology A* **2022**, *40* (2). DOI: 10.1116/6.0001658 (acccessed 5/31/2024).
(55) Nørskov, J. K.; Bligaard, T.; Logadottir, A.; Bahn, S.; Hansen, L. B.; Bollinger, M.; Bengaard, H.; Hammer, B.; Sljivancanin, Z.; Mavrikakis, M.; et al. Universality in

Heterogeneous Catalysis. *Journal of Catalysis* **2002**, *209* (2), 275-278. DOI: https://doi.org/10.1006/jcat.2002.3615.
(56) Gossenberger, F.; Roman, T.; Groß, A. Equilibrium coverage of halides on metal electrodes. *Surface Science* **2015**, *631*, 17-22. DOI: https://doi.org/10.1016/j.susc.2014.01.021.
(57) Gossenberger, F.; Juarez, F.; Gross, A. Sulfate, Bisulfate, and Hydrogen Co-adsorption on Pt(111) and Au(111) in an Electrochemical Environment. *Frontiers in Chemistry* **2020**, *8*. DOI: 10.3389/fchem.2020.00634.
(58) Groß, A. Reversible vs Standard Hydrogen Electrode Scale in Interfacial Electrochemistry from a Theoretician's Atomistic Point of View. *The Journal of Physical Chemistry C* **2022**, *126* (28), 11439-11446. DOI: 10.1021/acs.jpcc.2c02734.
(59) Kresse, G.; Furthmüller, J. Efficient iterative schemes for ab initio total-energy calculations using a plane-wave basis set. *Physical Review B* **1996**, *54* (16), 11169-11186. DOI: 10.1103/PhysRevB.54.11169.
(60) Press, W. H. *Numerical Recipes 3rd Edition: The Art of Scientific Computing*; Cambridge University Press, 2007.
(61) Blöchl, P. E. Projector augmented-wave method. *Physical Review B* **1994**, *50* (24), 17953-17979. DOI: 10.1103/PhysRevB.50.17953.
(62) Hammer, B.; Hansen, L. B.; Nørskov, J. K. Improved adsorption energetics within density-functional theory using revised Perdew-Burke-Ernzerhof functionals. *Physical Review B* **1999**, *59* (11), 7413-7421. DOI: 10.1103/PhysRevB.59.7413.
(63) Grimme, S.; Antony, J.; Ehrlich, S.; Krieg, H. A consistent and accurate ab initio parametrization of density functional dispersion correction (DFT-D) for the 94 elements H-Pu. *The Journal of Chemical Physics* **2010**, *132* (15). DOI: 10.1063/1.3382344 (acccessed 11/14/2023).
(64) Grimme, S. Density functional theory with London dispersion corrections. *WIREs Computational Molecular Science* **2011**, *1* (2), 211-228. DOI: https://doi.org/10.1002/wcms.30.
(65) Grimme, S.; Hansen, A.; Brandenburg, J. G.; Bannwarth, C. Dispersion-Corrected Mean-Field Electronic Structure Methods. *Chemical Reviews* **2016**, *116* (9), 5105-5154. DOI: 10.1021/acs.chemrev.5b00533.
(66) Mahlberg, D.; Sakong, S.; Forster-Tonigold, K.; Groß, A. Improved DFT Adsorption Energies with Semiempirical Dispersion Corrections. *Journal of Chemical Theory and Computation* **2019**, *15* (5), 3250-3259. DOI: 10.1021/acs.jctc.9b00035.
(67) Aoki, M.; Amawashi, H. Dependence of band structures on stacking and field in layered graphene. *Solid State Communications* **2007**, *142* (3), 123-127. DOI: https://doi.org/10.1016/j.ssc.2007.02.013.
(68) Methfessel, M.; Paxton, A. T. High-precision sampling for Brillouin-zone integration in metals. *Physical Review B* **1989**, *40* (6), 3616-3621. DOI: 10.1103/PhysRevB.40.3616.
(69) Jäckle, M.; Helmbrecht, K.; Smits, M.; Stottmeister, D.; Groß, A. Self-diffusion barriers: possible descriptors for dendrite growth in batteries? *Energy & Environmental Science* **2018**, *11* (12), 3400-3407, 10.1039/C8EE01448E. DOI: 10.1039/C8EE01448E.
(70) Jorgensen, W. L.; Tirado-Rives, J. The OPLS [optimized potentials for liquid simulations] potential functions for proteins, energy minimizations for crystals of cyclic peptides and crambin. *Journal of the American Chemical Society* **1988**, *110* (6), 1657-1666. DOI: 10.1021/ja00214a001.
(71) Berendsen, H. J. C.; Grigera, J. R.; Straatsma, T. P. The missing term in effective pair potentials. *The Journal of Physical Chemistry* **1987**, *91* (24), 6269-6271. DOI: 10.1021/j100308a038.